

## Microstructure and hydrogen storage properties of $V_{40}Ti_{20}Cr_{32}Fe_8$ alloy by heat treatment

Maohua Rong<sup>1,2</sup>, Gang Fu<sup>1</sup>, Feng Wang<sup>1,3</sup>, Jiang Wang<sup>1,2,a</sup>, Zhongmin Wang<sup>1,2</sup>, Guanghui Rao<sup>1,2</sup> and Huaiying Zhou<sup>1,2</sup>

<sup>1</sup>School of Material Science and Engineering, Guilin University of Electronic Technology, Guilin, Guangxi, China

<sup>2</sup>Guangxi Key Laboratory of Information Materials, Guilin University of Electronic Technology, Guilin, Guangxi, China

<sup>3</sup>School of Materials Science and Engineering, Beihang University, Beijing, China

**Abstract.** The microstructure, crystal structure, hydrogen storage properties and thermal stabilities of as-cast and annealed  $V_{40}Ti_{20}Cr_{32}Fe_8$  alloy prepared by arc-melting were studied in this work. It was confirmed that both as-cast and annealed (973 K/72 hrs)  $V_{40}Ti_{20}Cr_{32}Fe_8$  alloys are body-centered cubic (bcc) main phase and C14-typed Laves secondary ( $Cr_2Ti$ ). Experiment results show that the maximum hydrogen absorption capacities of as-cast  $V_{40}Ti_{20}Cr_{32}Fe_8$  alloy at 303 K, 333 K and 363 K are about 2.25 wt.%, 1.75 wt.% and 1.12 wt.%, while that of the annealed alloy at 303 K, 333 K and 363 K are about 2.26 wt.%, 1.76 wt.% and 1.26 wt.%, respectively. The maximum hydrogen desorption capacities of as-cast  $V_{40}Ti_{20}Cr_{32}Fe_8$  alloy at 303 K, 333 K and 363 K are about 1.15 wt.%, 0.89 wt.% and 0.60 wt.%, while that of the annealed alloy at 303 K, 333 K and 363 K are about 1.22 wt.%, 0.90 wt.% and 0.61 wt.%, respectively. It is indicated that hydrogen absorption/desorption kinetics of the V-Ti-Cr-Fe alloy is greatly improved by heat treatment.

**Keywords:** Ti-V-Cr-Fe alloys, hydrogen storage, thermal stability.

## 1 Introduction

V-Ti-based hydrogen storage alloys are considered to be one of the excellent hydrogen storage materials due to their large hydrogen absorption capacity compared with  $AB_5/AB_2/AB$ -typed hydrogen storage alloys [1-5]. However, the industrial applications of V-Ti-based hydrogen storage alloys were restricted due to poor kinetic characteristics, low hydrogen desorption capacity at room temperature and high costs [6-9]. The effective method of reducing their costs and improving the hydrogen storage properties is the addition of Cr and Fe elements into the V-Ti-based alloys [10-13].

It was reported that Cr or Fe could significantly affect hydrogen storage properties of V-Ti-based alloys [14-20]. Yan et al. [21] studied the higher hydrogen desorption capacities were 2.12 wt.% and 2.23 wt.% for  $V_{42}Ti_{28}Cr_{21.7}Fe_{8.3}$  and  $V_{55}Ti_{21.2}Cr_{17.1}Fe_{6.4}$  alloys at 298 K, respectively.  $Ti_{1.9}CrVFe_{0.1}$  alloy found by Kumar et al. [22] to absorb maximum 3.80 wt.% of hydrogen at room temperature. On the other hand, it has been understood that heat treatment could influence significantly hydrogen storage properties of V-Ti based alloys especially for kinetic property. Zhou et al. [23] found that the hydrogen desorption capacity of  $V_{35}Ti_{20}Cr_{45}$  alloy annealed at 973 K for 72 hrs is about 2.64 wt% at 303 K. Cho et al. [24] reported the large hydrogen desorption capacity of  $V_{25}Ti_{32}Cr_{43}$  alloy was 2.3

<sup>a</sup> Corresponding author: waj124@guet.edu.cn, wangjiang158@163.com

wt% at 303 K after heat treatment at 1653 K for 1 min. Okada et al. [25] found that the hydrogen desorption capacity of  $V_{35}Ti_{25}Cr_{40}$  alloy annealed at 1573 K for 1 min was about 2.6 wt.% at 313 K. However, the effect of heat treatment on hydrogen storage properties of Ti-V based alloys still needs to be investigated further to optimize heat treatment process including annealed temperature and time to improve kinetic characteristics and hydrogen absorption/desorption capacities.

The purpose of the present work was to examine the microstructure, crystal structure, thermal stability and hydrogen storage properties of  $V_{40}Ti_{20}Cr_{32}Fe_8$  alloy using X-ray diffraction (XRD), Scanning Electron Microscopy (SEM), differential scanning calorimeter (DSC) and Sievert-type apparatus (Sateram PCTpro2000), respectively. The effect of heat treatment on kinetic characteristics (absorption/desorption) and thermal stability of the alloy was thus discussed.

## 2 Experimental procedures

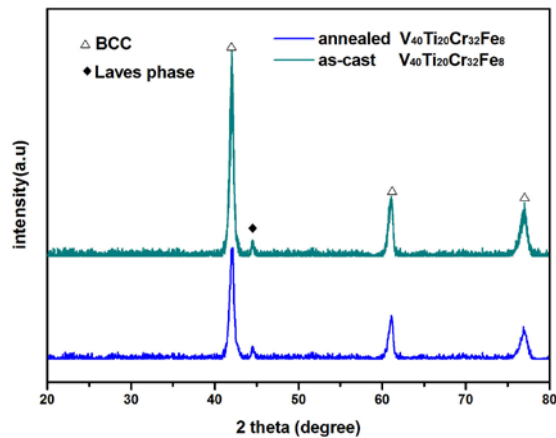
V (99.99 % purity), Ti (99.99 % purity), Fe (99.99 % purity) Cr (99.99 % purity) were used as the starting materials. Ingots with nominal composition of  $V_{40}Ti_{20}Cr_{32}Fe_8$  alloy were prepared by arc melting pure elements in an arc furnace using a non-consumable tungsten electrode under an inert argon atmosphere. Ingots were re-melted more than four times to homogenize the alloy composition with a total mass loss of less than 1%.

The crystal structure and microstructure of alloy samples were examined by X-ray diffraction (XRD, Cu K $\alpha$  radiation) and Scanning Electron Microscope (SEM) with Energy Dispersive X-ray Spectrometers (EDS). The hydrogen kinetic curves and temperature programmed desorption (TPD) curves were measured using Sievert-type apparatus (PCTpro2000). Thermal stability of the alloys was measured by differential scanning calorimeter (DSC, Netzsch STA449 F3) under a flowing pure argon atmosphere at different heating rates of 10 K/min. For activation process, the powder smashed from as-cast alloys were put into the reactor firstly and evacuated for 15 min at 298 K, and then hydrogen was introduced gradually into the reactor up to a pressure of 2 MPa for the absorption process. Finally, the next hydrogen absorption process would begin after the reactor was heated to 573 K and evacuated for 60 min. The measurements of hydrogen kinetic characteristics were carried out at 303 K, 333K and 363 K, respectively. This desorption process was performed with a heating rate of 5 K/min from 300 K to 578 K during TPD testing.

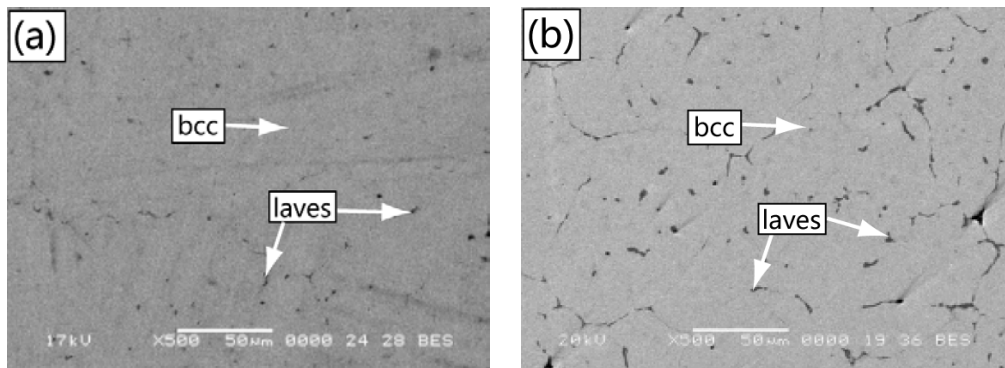
## 3 Results and discussion

Figure 1 shows the powder XRD patterns of as-cast and annealed  $V_{40}Ti_{20}Cr_{32}Fe_8$  alloy. As can be seen, the main intensity peaks could be indexed as the bcc main phase and the C14-typed Laves secondary phase (Cr<sub>2</sub>Ti) in  $V_{40}Ti_{20}Cr_{32}Fe_8$  alloys. The intensity of diffraction peak enhances and the width of the peak could be much weaker for bcc phase and C14-typed Laves after heat treatment at (973K/72hrs), which implies that heat treatment promotes the crystallization of the bcc phase and C14-typed Laves.

The alloy was also examined by SEM as shown in Figure 2. The Back Scatter Electron (BSE) images of  $V_{40}Ti_{20}Cr_{32}Fe_8$  alloy show that both as-cast and annealed alloys are bcc main phase with the C14-typed Laves phase. According to EDS measurements, the as-cast has the main phase (the grey phase, 44.0 at.% V, 15.5 at.% Ti, 33.5 at.% Cr, 7.0 at.% Fe,) with the secondary phase (the dark phase, 24.2 at.% V, 37.2 at.% Ti, 34.5 at.% Cr, 4.1 at.% Fe). The annealed alloy has the main phase (the grey phase, 44.9 at.% V, 14.8 at.% Ti, 32.7 at.% Cr, 7.6 at.% Fe,) with the secondary phase (the dark phase, 23.1 at.% V, 38.3 at.% Ti, 33.5 at.% Cr, 5.1 at.% Fe). Moreover, the content of C14-typed Laves phase increases after annealing. It indicates the SEM results are in good agreements with XRD results.



**Figure 1.** XRD patterns of as-cast and annealed  $V_{40}Ti_{20}Cr_{32}Fe_8$  alloys.



**Figure 2.** BSE Micrographs of as-cast and annealed  $V_{40}Ti_{20}Cr_{32}Fe_8$  alloys.

Figure 3 and Figure 4 are the kinetic curves of hydrogen absorption/desorption of as-cast and annealed  $V_{40}Ti_{20}Cr_{32}Fe_8$  alloys at 303 K, 333 K and 363 K after being activated fully at different temperatures under the hydrogen pressure of 2 MPa/vacuum, respectively. The maximum hydrogen absorption capacities of as-cast  $V_{40}Ti_{20}Cr_{32}Fe_8$  alloy at 303 K, 333 K and 363 K are about 2.25 wt.%, 1.75 wt.% and 1.12 wt.% in Figure 3(a), while that of the annealed alloy at 303 K, 333 K and 363 K are about 2.26 wt.%, 1.76 wt.% and 1.26 wt.% in Figure 3(b), respectively. Moreover, it is interestingly noted that the as-cast  $V_{40}Ti_{20}Cr_{32}Fe_8$  alloy takes  $\sim 1500$  s to reach the maximum hydrogen absorption capacity at 303 K in Figure 3(a), while it takes only  $\sim 250$  s to reach the maximum hydrogen absorption capacity after heat treatment in Figure 3(b). The maximum hydrogen desorption capacities of as-cast  $V_{40}Ti_{20}Cr_{32}Fe_8$  alloy at 303 K, 333 K and 363 K are about 1.15 wt.%, 0.89 wt.% and 0.60 wt.% in Figure 4(a), while that of the annealed alloy at 303 K, 333 K and 363 K are about 1.22 wt.%, 0.90 wt.% and 0.61 wt.% in Figure 4(b), respectively. In addition, it is noticed that the as-cast  $V_{40}Ti_{20}Cr_{32}Fe_8$  alloy takes  $\sim 650$  s to reach the maximum hydrogen desorption capacity at 303 K in Figure 4(a), while it takes only  $\sim 250$  s to reach the maximum hydrogen desorption capacity after heat treatment in Figure 4(b). Therefore, the hydrogen absorption/desorption kinetic properties of the as-cast alloy after heat treatment become much well. The reason could be due to the more content of C14-typed Laves secondary phase in the bcc matrix phase after annealing, which could help hydrogen atom to penetrate more rapidly through the bulk because of the presence of grain boundaries. The reason mentioned above was also employed by Zhou et al. [23] to explain the improvement of the activation properties in  $V_{35}Ti_{20}Cr_{45}$  alloy.

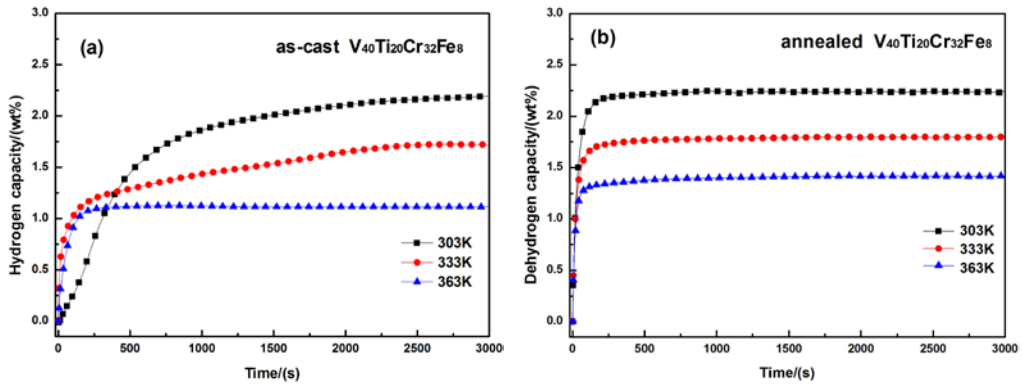


**Figure 3.** Kinetic curves of hydrogen absorption of as-cast and annealed  $V_{40}Ti_{20}Cr_{32}Fe_8$  alloy at 303 K, 333 K and 363 K. (a) as-casting and (b) annealed.

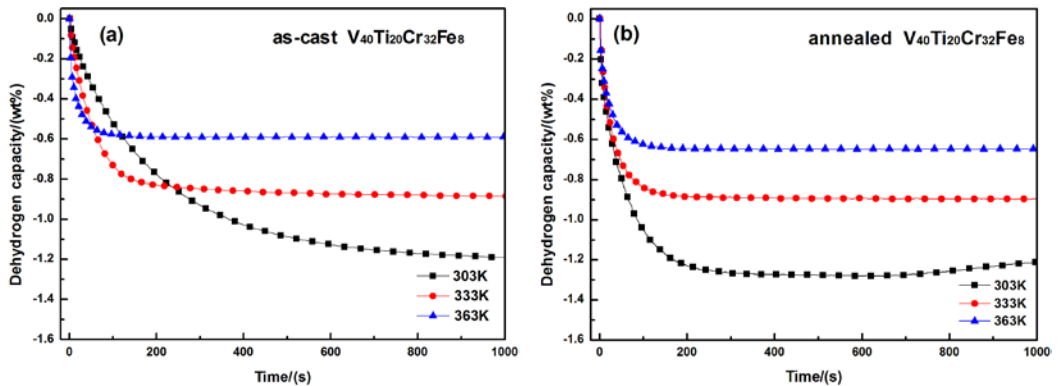


**Figure 4.** Kinetic curves of hydrogen desorption of as-cast and annealed  $V_{40}Ti_{20}Cr_{32}Fe_8$  alloy at 303 K, 333 K and 363 K. (a) as-casting and (b) annealed.

In order to examine the hydrogen desorption process of  $V_{40}Ti_{20}Cr_{32}Fe_8$  alloy, DSC measurements of as-cast and annealed alloys after full absorption were performed at 10 K/min heating rates under a continuous argon flow from 450 K to 850 K as shown in Figure 5. As can be seen, there are two endothermic peaks in annealed alloy at 585 K and 680 K, respectively, while two endothermic peaks in as-cast alloy are 596 K and 697 K. It is noticeable that the dehydrogenation temperature of the annealed alloy is lower than that of the as-cast alloy, which is in good agreement with hydrogen absorption/desorption kinetic characteristic mentioned above.

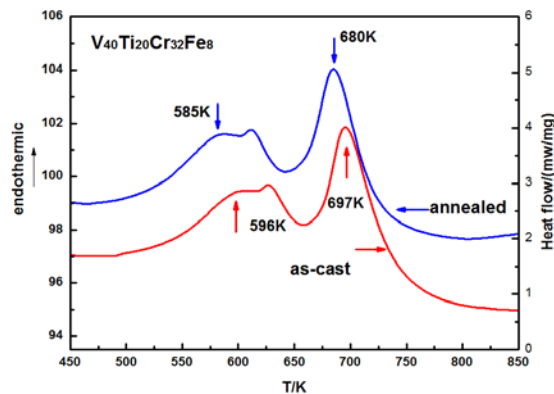


**Figure 5.** DSC curves of hydrogenated as-cast and annealed  $V_{40}Ti_{20}Cr_{32}Fe_8$  alloy.

In addition, TPD measurements of as-cast and annealed  $V_{40}Ti_{20}Cr_{32}Fe_8$  alloys after full absorption were performed at 5 K/min from 300 K to 578 K as shown in Figure 6. As can be seen, the hydrogen desorption process of as-cast and annealed alloys could be carried out. The hydrogen desorption capacities are improved with increasing temperature. The hydrogen desorption capacities of as-cast  $V_{40}Ti_{20}Cr_{32}Fe_8$  is about 1.61 wt.% at 573 K, while that of annealed alloy is about 1.60 wt.% at 573 K. TPD results are in good agreements with the comparison of kinetic properties of as-cast and annealed alloy, which show that the hydrogen absorption/desorption kinetics of the annealed alloy is improved greatly.

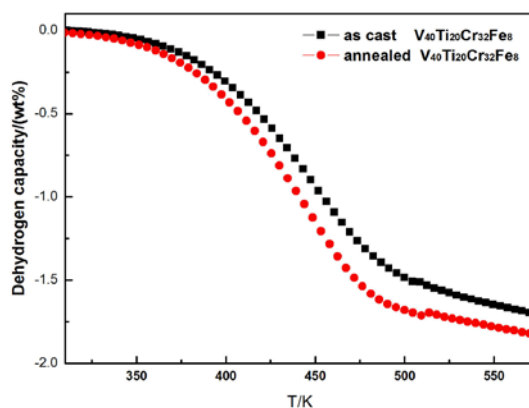


**Figure 6.** TPD curves of hydrogenated as-cast and annealed  $V_{40}Ti_{20}Cr_{32}Fe_8$  alloy.

## 4 Conclusions

In this work, the crystal structure, microstructure, hydrogen storage properties and thermal stabilities of  $V_{40}Ti_{20}Cr_{32}Fe_8$  alloys were studied using XRD, SEM and Sievert-type apparatus, respectively. The following conclusions could be drawn:

(1) The SEM and XRD results show that both as-cast and annealed  $V_{40}Ti_{20}Cr_{32}Fe_8$  alloys are body-centered cubic (bcc) and the C14-typed Laves secondary phase.

(2) The maximum hydrogen absorption capacities of as-cast  $V_{40}Ti_{20}Cr_{32}Fe_8$  alloy at 303 K, 333 K and 363 K are about 2.25 wt.%, 1.75 wt.% and 1.12 wt.%, while that of the annealed alloy at 303 K, 333 K and 363 K are about 2.26 wt.%, 1.76 wt.% and 1.26 wt.%, respectively.

The maximum hydrogen desorption capacities of as-cast  $V_{40}Ti_{20}Cr_{32}Fe_8$  alloy at 303 K, 333 K and 363 K are about 1.15 wt.%, 0.89 wt.% and 0.60 wt.%, while that of the annealed alloy at 303 K, 333 K and 363 K are about 1.22 wt.%, 0.90 wt.% and 0.61 wt.%, respectively. It is indicated that kinetic properties of the annealed V-Ti-Cr-Fe alloy would be better.

## Acknowledgements

This work was financially supported by the Joint Foundation of Guilin University of Electronic Technology and Guilin Electrical Equipment Scientific Research Institute (Project No. 20141103-08-Z) and Guangxi Natural Science Foundation (Grant No. 2014GXNSFBA118235). The authors also acknowledge National Natural Science Foundation of China (Grant No. 51461013) for financial support.

## References

1. Z.W. Chen, X.Z. Xiao, L.X. Chen, X.L. Fan, L.X. Liu et al., J Alloys Compd, **585**, 307-311(2014).

2. L. Schlapbach, A. Züttler, *Nature*, **414**, 353-358 (2001).
3. S.J. Qiu, J.L. Huang, Y.J. Zou, C.L. Xiang, H.Z. Zhang, F. Xu, L.X. Sun, H.Y. Zhou, *J. Alloys Compd*, **648**, 320-325 (2015).
4. Z.Y. Yang, X.H. Zeng, W. Cai, *Scripta Mater*, **99**, 97-100 (2015).
5. P. Chen, M. Zhu, *Mater. Today*, **11**, 37-43 (2008).
6. J.B. Zhu, L. Q. Ma, F. Liang, L.M. Wang, *Int. J. Hydrogen Energy*, **40**, 6860-6865 (2015).
7. A. Guéguen, M. Latroche, *J. Alloys Compd*, **509**, 5562-5566 (2011).
8. S. Suwarno, J.K. Solberg, J.P. Maehlen, B. Krogh, V.A. Yartys, *Int. J. Hydrogen Energy*, **377**, 624-628 (2012).
9. L.D. Pickering, D. Reed, A.I. Bevan, D. Book, *J. Alloy Compd*, **645**, S400-S403 (2015).
10. L. Pickering, J. Li, D. Reed, A.I. Bevan, *J. Alloys Compd*, **580**, 233-237 (2013).
11. Z.M. Hang, X.Z. Xiao, Li, Z. Tan, Z.H. He, H.W. Ge, C.P. Chen, L.X. Chen, *J. Alloys Compd*, **529**, 128-133 (2012).
12. T. Kuriwa, T. Maruyama, A. Kamegawa, M. Okada, *Int. J. Hydrogen Energy*, **35**, 9082-9087, (2010).
13. L. Pickering, J. Li, D. Reed, A.I. Bevan, D. Book, *J. Alloys Compd*, **529**, 128-133 (2012).
14. Z. Hang, X. Xiao, K. Yu, S. Li, C. Chen, L. Chen, *Int. J. Hydrogen Energy* **35**, 8143-8148 (2010).
15. G. Fu, F. Wang, J. Wang, M.H. Rong, Z.M. Wang, G.H. Rao, H.Y. Zhou, *Mater. Sci. Forum*, **847**, 3-7 (2016).
16. U. Ulmer, K. Asano, T. Bergfeldt, V.S.K. Chakravadhanula, R. Dittmeyer, H. Enoki, C. Kübel, Y. Nakamura, A. Pohl, M. Fichtner, *Int. J. Hydrogen Energy*, **39**, 20000-20008 (2014).
17. R. Jeng, C.Y. Chou, S.L. Lee, Y.C. Wu, H.Y. Bor, *Chin. Inst. Eng*, **34**, 601-608 (2011).
18. C. Wu, A. Borgschulte, U. Frischknecht, Y. Yan, F. Yang, L. Luo, Y. Chen, A. Züttler, *J. Alloys Compd*, **580**, 156-158 (2013).
19. V.I. Chizhik, I.A. Rykov, M.G. Shelyapina, D. Fruchart, *Int. J. Hydrogen Energy*, **39**, 17416-17421 (2014).
20. M.X. Gao, H. Miao, Y. Zhao, Y.F. Liu, H.G. Pan, *J. Alloys Compd*, **484**, 249-255 (2009).
21. Y.G. Yan, Y.G. Chen, H. Liang, X.X. Zhou, C.L. Wu, M.D. Tao, L.J. Pang, *J. Alloys Compd*, **454**, 427-431. (2008).
22. A. Kumar, S. Banerjee, C.G. Pillai, *Int. J. Hydrogen Energy*, **38**, 3024-3029, (2013).
23. H.Y. Zhou, F. Wang, J. Wang, Z.M. Wang, Q.R. Yao, J.Q. Deng, C.Y. Tang, G.H. Rao, *Int. J. Hydrogen Energy*, **39**, 14887-14895 (2014).
24. W. Cho, G. Shim, G.S. Choi, C.N. Park, J.H. Yoo, J. Choi, *J. Alloys Compd*, **32**, 2977-2981 (2007).
25. M. Okada, T. Kuriwa, T. Tamura, H. Takamura, A. Kamegawa, *J. Alloys Compd*, **330**, 511-516 (2002).